International Journal of Geographical Information Science
Vol. 23, No. 2, February 2009, 213–231

Research Article

Computation of the third-order partial derivatives from a digital elevation model

IGOR V. FLORINSKY
Institute of Mathematical Problems of Biology, Russian Academy of Sciences, Pushchino, Moscow Region 142290, Russia

(*Received 19 July 2007; in final form 1 October 2008*)

Loci of extreme curvature of the topographic surface may be defined by the derivation function (T) depending on the first-, second-, and third-order partial derivatives of elevation. The loci may partially describe ridge and thalweg lines. The first- and second-order partial derivatives are commonly calculated from a digital elevation model (DEM) by fitting the second-order polynomial to a 3×3 window. This approach cannot be used to compute the third-order partial derivatives and T. We deduced formulae to estimate the first-, second-, and third-order partial derivatives from a DEM fitting the third-order polynomial to a 5×5 window. The polynomial is approximated to elevation values of the window. This leads to a local denoising that may enhance calculations. Under the same grid size of a DEM and root mean square error (RMSE) of elevation, calculation of the second-order partial derivatives by the method developed results in significantly lower RMSE of the derivatives than that using the second-order polynomial and the 3×3 window. An RMSE expression for the derivation function is deduced. The method proposed can be applied to derive any local topographic variable, such as slope gradient, aspect, curvatures, and T. Treatment of a DEM by the method developed demonstrated that T mapping may not substitute regional logistic algorithms to detect ridge/thalweg networks. However, the third-order partial derivatives of elevation can be used in digital terrain analysis, particularly, in landform classifications.

Keywords: Digital terrain modelling; Surface; Curvature; Drainage network

1. Introduction

Let us consider a portion of the topographic surface which is: (1) considerably less than the Earth's radius, (2) characterised by homogeneous gravity, and (3) described by a single-valued infinitely differentiable function $z=f(x, y)$, where z is elevation, x and y are Cartesian co-ordinates. One can distinguish two families of spatial curves on the topographic surface: contours and slope lines (Cayley 1859). A contour is a locus of intersection of a horizontal plane with the topographic surface. For any point of a slope line, the direction of a tangent vector to the curve coincides with the direction of a tangential component of the gravity vector. Slope lines are not defined at special points of the surface (e.g., local maxima, minima, saddles, flat areas). Slope lines and contours are mutually perpendicular at their intersections.

*Corresponding author. Email: iflorinsky@yahoo.ca

International Journal of Geographical Information Science
ISSN 1365-8816 print/ISSN 1362-3087 online
http://www.tandf.co.uk/journals
DOI: 10.1080/13658810802527499

Considering these families of spatial curves, one can distinguish two groups of loci of extreme curvature of the topographic surface: (1) locus of extreme curvature of contours, and (2) locus of extreme curvature of slope lines. Obviously extreme curvature varies in sign: one can set the positive sign to convex areas and negative – to concave ones. Loci of extreme curvature may *partially* describe four types of geomorphic lines:

- Ridge lines, or crests – the locus of positive extreme curvature of contours.
- Valley lines, or thalwegs – the locus of negative extreme curvature of contours.
- Convex break lines – the locus of positive extreme curvature of slope lines.
- Concave break lines – the locus of negative extreme curvature of slope lines.

Geomorphic 'lines' are formed not only by the loci of extreme curvature, but by loci of special points (i.e., local maxima and minima, saddles, and flat horizontal areas) as well.

At the same time, one can consider ridge and valley lines as two topologically connected tree- or graph-like hierarchical structures. Maxwell (1870) defined a ridge as a slope line connecting a sequence of local maximal and saddle points, while a thalweg as a slope line connecting a sequence of local minimal and saddle points. Over a century, these quantitative definitions have provided a basis for manual delineation of ridge and valley lines using topographic maps.

Digital terrain modelling (Florinsky 1998b, Shary *et al.* 2002) is closely allied to signal processing (Florinsky 2002). There is a principle difference between a topographic surface, with properties that are in many respects controlled by gravity, and an image intensity function. However, from the technical point of view, the algorithms of digital terrain modelling may be applied in image processing, and vice versa, algorithms of image processing are used in digital terrain analysis. Thus, it is not surprising that delineation of ridges and thalwegs is one of the topical tasks of digital terrain modelling, image processing, and machine vision. In digital terrain modelling, researchers focus attention on the detection of thalwegs. The delineation of ridges receives much consideration in image processing.

The twofold nature of geomorphic lines is responsible for the existence of two fundamentally different groups of techniques to delineate ridges and thalwegs. Methods of the first group are based on principles of differential geometry. Originating in classical works on geometry (de Saint-Venant 1852, Boussinesq 1871, Jordan 1872, Breton de Champ 1877), they are predominantly used in image processing (Haralick 1983, Koenderink and van Doorn 1993, Eberly *et al.* 1994, Maintz *et al.* 1996, Rieger 1997, López *et al.* 1998). In these approaches, differential geometric criteria are usually applied to detect loci of extreme values of mean, principal, and contour curvatures. A non-trivial method by López and Serrat (1996), implementing a differential equation of Rothe (1915), may be also placed into this group.

Methods of the second group are based on logistic processing of data, such as cell-to-cell flow routing and calculation of an upslope catchment area with subsequent thresholding of its values. These approaches are commonly used in digital terrain modelling (Mark 1984, O'Callaghan and Mark 1984, Band 1986, Douglas 1986, Skidmore 1990, Tribe 1992, Meisels *et al.* 1995, Chang *et al.* 1998, Jones 2002).

In scale terms, methods of the first group are local since they concern a small neighbourhood of a point within a moving window. Methods of the second group are regional or global because determination of flow routing requires an analysis of rather large portions of a terrain.

There is a third group of algorithms combining local differential geometric and regional logistic approaches. In this case, differential geometrical criteria are used to

detect saddle points or points of extreme contour curvature, and then logistic procedures are applied to link the points for visualisation of ridges and thalwegs (Gauch and Pizer 1993, Kweon and Kanade 1994, Steger 1999).

Horizontal curvature (k_h) is the measure of convergence and divergence of slope lines. Negative values of k_h indicate convergence areas of slope lines, while positive values of k_h correspond to divergence areas. At the same time, k_h is the product of the contour curvature and slope factor (Shary *et al.* 2002). This means that k_h contains information on the behaviour of both contours and slope lines. Thus, to find loci of extreme curvature of both families of spatial curves, one needs to find loci of extreme values of k_h. Clearly, they correspond to zero values of the k_h derivative, the so-called derivation function (T) (Shary and Stepanov 1991):

$$T = \frac{\mathrm{d}k_h}{\mathrm{d}\xi} \tag{1}$$

where ξ is a length of a contour arc, and

$$k_h = -\frac{q^2 r - 2pqs + p^2 t}{(p^2+q^2)\sqrt{1+p^2+q^2}} \tag{2}$$

where r, t, s, p and q are the second- and first-order partial derivatives of elevation:

$$r = \frac{\partial^2 z}{\partial x^2},\ t = \frac{\partial^2 z}{\partial y^2},\ s = \frac{\partial^2 z}{\partial x \partial y},\ p = \frac{\partial z}{\partial x},\ q = \frac{\partial z}{\partial y} \tag{3a}$$

The expression for the derivation function has the following form (Appendix A):

$$T = \frac{1}{\sqrt{(p^2+q^2)^3(1+p^2+q^2)}}\left\{q^3 a - 3pq^2 b + 3p^2 qc - p^3 d + \frac{(q^2 r - 2pqs + p^2 t)\left[pq(t-r) + s(p^2-q^2)\right](2+3p^2+3q^2)}{(p^2+q^2)(1+p^2+q^2)}\right\} \tag{4}$$

where a, d, b and c are the third-order partial derivatives of elevation:

$$a = \frac{\partial^3 z}{\partial x^3},\ d = \frac{\partial^3 z}{\partial y^3},\ b = \frac{\partial^3 z}{\partial x^2 \partial y},\ c = \frac{\partial^3 z}{\partial x \partial y^2} \tag{3b}$$

T can be interpreted as a measure for the deflection of k_h from loci of extreme curvature of the topographic surface. The unit of T is m^{-2}. Shary and Stepanov (1991) proposed that ridges and convex break lines relate to the locus of $T=0$ within divergence areas, while thalwegs and concave break lines correspond to the locus of $T=0$ within convergence areas.

One can calculate r, t, s, p and q from a square-spaced digital elevation model (DEM) by various methods. The method of Evans (1979) has received wide acceptance owing to high accuracy (Florinsky 1998a, Schmidt *et al.* 2003). Under this method, the second-order polynomial is fitted by least squares to a 3×3 square-gridded window leading to finite difference formulae of r, t, s, p, and q (Appendix B). Using a partial quartic polynomial and a 3×3 window, Zevenbergen and Thorne (1987) developed formulae of polynomial coefficients proportional to b and c, but did not utilise them.

As far as we know, finite difference expressions for the third-order partial derivatives, and T mapping to detect loci of extreme curvature have not been previously reported. In this paper, these formulae are deduced, and T computation from a DEM is presented. Calculation accuracy of the partial derivatives of elevation and T is discussed. We also check a proposal of Shary and Stepanov (1991) that T mapping can be used to reveal ridge and thalweg networks.

2. Formulae for the third-order partial derivatives

It is clear that the second-order polynomial (A6) is not suitable to deduce formulae of third-order partial derivatives because it does not include third-order terms. There is a need to utilise, at least, the third-order polynomial. Using the well-known Taylor's formula (Fikhtengolts 1966, Lang 1996), a function $z=f(x, y)$ can be expressed conveniently as follows:

$$z=\frac{1}{6}ax^3+\frac{1}{6}dy^3+\frac{1}{2}bx^2y+\frac{1}{2}cxy^2+\frac{1}{2}rx^2+\frac{1}{2}ty^2+sxy+px+qy+u \qquad (5)$$

Under the least squares method (Bjerhammar 1973), one should carry out n measurements of z to find m unknown coefficients of $z=f(x, y)$, with $n>(m+1)$. Therefore, one cannot use a 3×3 window (Appendix B) to find the ten unknown coefficients a, d, b, c, r, t, s, p, q and u of the third-order polynomial (5): the window includes only nine measured values of z. To find these coefficients for the central point of a window, there is a need to use, at least, a 5×5 window (figure 1). Cartesian coordinates and elevations of the land surface are known for twenty five points of this window: $(-2w, 2w, z_1)$, $(-w, 2w, z_2)$, $(0, 2w, z_3)$, $(w, 2w, z_4)$, $(2w, 2w, z_5)$, $(-2w, w, z_6)$, $(-w, w, z_7)$, $(0, w, z_8)$, (w, w, z_9), $(2w, w, z_{10})$, $(-2w, 0, z_{11})$, $(-w, 0, z_{12})$, $(0, 0, z_{13})$, $(w, 0, z_{14})$, $(2w, 0, z_{15})$, $(-2w, -w, z_{16})$, $(-w, -w, z_{17})$, $(0, -w, z_{18})$, $(w, -w, z_{19})$, $(2w, -w, z_{20})$, $(-2w, -2w, z_{21})$, $(-w, -2w, z_{22})$, $(0, -2w, z_{23})$, $(w, -2w, z_{24})$, and $(2w, -2w, z_{25})$.

Let us fit the polynomial (5) to the 5×5 window by the least squares method (Bjerhammar 1973). Writing the polynomial (5) for all points of the window, we obtain a system of twenty five conditional linear equations:

$$\boldsymbol{\alpha}=\mathbf{F}\boldsymbol{\beta} \qquad (6)$$

where $\boldsymbol{\alpha}$ is a 25×1 matrix of twenty five measured values of z:

$$\boldsymbol{\alpha}=\begin{Vmatrix} z_1 \\ z_2 \\ \vdots \\ z_{25} \end{Vmatrix} \qquad (7)$$

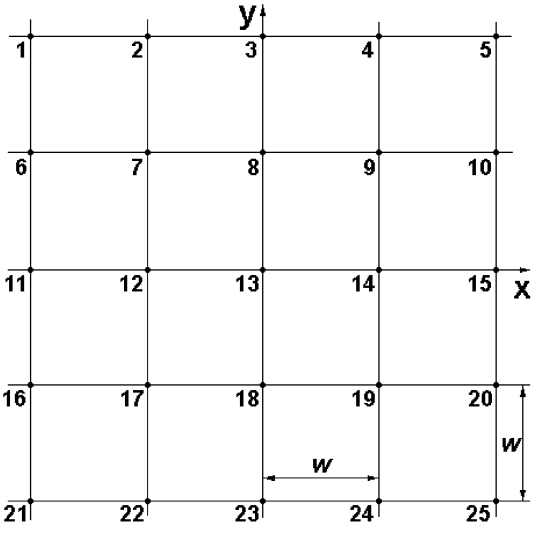

Figure 1. The 5×5 window: 1, …, 25 are numbers of the window nodes, w is grid size (metres).

$\boldsymbol{\beta}$ is a 10×1 matrix of ten unknown coefficients of the polynomial (5):

$$\boldsymbol{\beta} = \begin{Vmatrix} a \\ d \\ b \\ c \\ r \\ t \\ s \\ p \\ q \\ u \end{Vmatrix} \tag{8}$$

and $\mathbf{F}$ is a 25×10 matrix of known coefficients of the equation system:

$$\mathbf{F} = \begin{Vmatrix}
-\frac{4}{3}w^3 & \frac{4}{3}w^3 & 4w^3 & -4w^3 & 2w^2 & 2w^2 & -4w^2 & -2w & 2w & 1 \\
-\frac{1}{6}w^3 & \frac{4}{3}w^3 & w^3 & -2w^3 & \frac{1}{2}w^2 & 2w^2 & -2w^2 & -w & 2w & 1 \\
0 & \frac{4}{3}w^3 & 0 & 0 & 0 & 2w^2 & 0 & 0 & 2w & 1 \\
\frac{1}{6}w^3 & \frac{4}{3}w^3 & w^3 & 2w^3 & \frac{1}{2}w^2 & 2w^2 & 2w^2 & w & 2w & 1 \\
\frac{4}{3}w^3 & \frac{4}{3}w^3 & 4w^3 & 4w^3 & 2w^2 & 2w^2 & 4w^2 & 2w & 2w & 1 \\
-\frac{4}{3}w^3 & \frac{1}{6}w^3 & 2w^3 & -w^3 & 2w^2 & \frac{1}{2}w^2 & -2w^2 & -2w & w & 1 \\
-\frac{1}{6}w^3 & \frac{1}{6}w^3 & \frac{1}{2}w^3 & -\frac{1}{2}w^3 & \frac{1}{2}w^2 & \frac{1}{2}w^2 & -w^2 & -w & w & 1 \\
0 & \frac{1}{6}w^3 & 0 & 0 & 0 & \frac{1}{2}w^2 & 0 & 0 & w & 1 \\
\frac{1}{6}w^3 & \frac{1}{6}w^3 & \frac{1}{2}w^3 & \frac{1}{2}w^3 & \frac{1}{2}w^2 & \frac{1}{2}w^2 & w^2 & w & w & 1 \\
\frac{4}{3}w^3 & \frac{1}{6}w^3 & 2w^3 & w^3 & 2w^2 & \frac{1}{2}w^2 & 2w^2 & 2w & w & 1 \\
-\frac{4}{3}w^3 & 0 & 0 & 0 & 2w^2 & 0 & 0 & -2w & 0 & 1 \\
-\frac{1}{6}w^3 & 0 & 0 & 0 & \frac{1}{2}w^2 & 0 & 0 & -w & 0 & 1 \\
0 & 0 & 0 & 0 & 0 & 0 & 0 & 0 & 0 & 1 \\
\frac{1}{6}w^3 & 0 & 0 & 0 & \frac{1}{2}w^2 & 0 & 0 & w & 0 & 1 \\
\frac{4}{3}w^3 & 0 & 0 & 0 & 2w^2 & 0 & 0 & 2w & 0 & 1 \\
-\frac{4}{3}w^3 & -\frac{1}{6}w^3 & -2w^3 & -w^3 & 2w^2 & \frac{1}{2}w^2 & 2w^2 & -2w & -w & 1 \\
-\frac{1}{6}w^3 & -\frac{1}{6}w^3 & -\frac{1}{2}w^3 & -\frac{1}{2}w^3 & \frac{1}{2}w^2 & \frac{1}{2}w^2 & w^2 & -w & -w & 1 \\
0 & -\frac{1}{6}w^3 & 0 & 0 & 0 & \frac{1}{2}w^2 & 0 & 0 & -w & 1 \\
\frac{1}{6}w^3 & -\frac{1}{6}w^3 & -\frac{1}{2}w^3 & \frac{1}{2}w^3 & \frac{1}{2}w^2 & \frac{1}{2}w^2 & -w^2 & w & -w & 1 \\
\frac{4}{3}w^3 & -\frac{1}{6}w^3 & -2w^3 & w^3 & 2w^2 & \frac{1}{2}w^2 & -2w^2 & 2w & -w & 1 \\
-\frac{4}{3}w^3 & -\frac{4}{3}w^3 & -4w^3 & -4w^3 & 2w^2 & 2w^2 & 4w^2 & -2w & -2w & 1 \\
-\frac{1}{6}w^3 & -\frac{4}{3}w^3 & -w^3 & -2w^3 & \frac{1}{2}w^2 & 2w^2 & 2w^2 & -w & -2w & 1 \\
0 & -\frac{4}{3}w^3 & 0 & 0 & 0 & 2w^2 & 0 & 0 & -2w & 1 \\
\frac{1}{6}w^3 & -\frac{4}{3}w^3 & -w^3 & 2w^3 & \frac{1}{2}w^2 & 2w^2 & -2w^2 & w & -2w & 1 \\
\frac{4}{3}w^3 & -\frac{4}{3}w^3 & -4w^3 & 4w^3 & 2w^2 & 2w^2 & -4w^2 & 2w & -2w & 1
\end{Vmatrix} \tag{9}$$

To determine unknown coefficients of the polynomial (5), we should solve the following equation:

$$\boldsymbol{\beta} = \left(\mathbf{F}^{\mathbf{T}}\mathbf{F}\right)^{-1}\mathbf{F}^{\mathbf{T}}\boldsymbol{\alpha} \tag{10}$$

where $\mathbf{F}^{\mathbf{T}}$ is a transposed matrix of $\mathbf{F}$, and $(\mathbf{F}^{\mathbf{T}}\mathbf{F})^{-1}$ is an inverse matrix of $\mathbf{F}^{\mathbf{T}}\mathbf{F}$. Through matrix operations, we can obtain the 10×25 matrix:

$$\left(\mathbf{F}^{\mathbf{T}}\mathbf{F}\right)^{-1}\mathbf{F}^{\mathbf{T}} = \begin{Vmatrix}
-\frac{1}{10w^3} & \frac{1}{5w^3} & 0 & -\frac{1}{5w^3} & \frac{1}{10w^3} & -\frac{1}{10w^3} & \frac{1}{5w^3} & 0 \\
\frac{1}{10w^3} & \frac{1}{10w^3} & \frac{1}{10w^3} & \frac{1}{10w^3} & \frac{1}{10w^3} & -\frac{1}{5w^3} & -\frac{1}{5w^3} & -\frac{1}{5w^3} \\
\frac{2}{35w^3} & -\frac{1}{35w^3} & -\frac{2}{35w^3} & -\frac{1}{35w^3} & \frac{2}{35w^3} & \frac{1}{35w^3} & -\frac{1}{70w^3} & -\frac{1}{35w^3} \\
-\frac{2}{35w^3} & -\frac{1}{35w^3} & 0 & \frac{1}{35w^3} & \frac{2}{35w^3} & \frac{1}{35w^3} & \frac{1}{70w^3} & 0 \\
\frac{2}{35w^2} & -\frac{1}{35w^2} & -\frac{2}{35w^2} & -\frac{1}{35w^2} & \frac{2}{35w^2} & \frac{2}{35w^2} & -\frac{1}{35w^2} & -\frac{2}{35w^2} \\
\frac{2}{35w^2} & \frac{2}{35w^2} & \frac{2}{35w^2} & \frac{2}{35w^2} & \frac{2}{35w^2} & -\frac{1}{35w^2} & -\frac{1}{35w^2} & -\frac{1}{35w^2} \\
-\frac{1}{25w^2} & -\frac{1}{50w^2} & 0 & \frac{1}{50w^2} & \frac{1}{25w^2} & -\frac{1}{50w^2} & -\frac{1}{100w^2} & 0 \\
\frac{31}{420w} & -\frac{11}{105w} & 0 & \frac{11}{105w} & -\frac{31}{420w} & -\frac{1}{84w} & -\frac{31}{210w} & 0 \\
-\frac{31}{420w} & \frac{1}{84w} & \frac{17}{420w} & \frac{1}{84w} & -\frac{31}{420w} & \frac{11}{105w} & \frac{31}{210w} & \frac{17}{105w} \\
-\frac{13}{175} & \frac{2}{175} & \frac{1}{25} & \frac{2}{175} & -\frac{13}{175} & \frac{2}{175} & \frac{17}{175} & \frac{22}{175}
\end{Vmatrix}$$

$$\begin{Vmatrix}
-\frac{1}{5w^3} & \frac{1}{10w^3} & -\frac{1}{10w^3} & \frac{1}{5w^3} & 0 & -\frac{1}{5w^3} & \frac{1}{10w^3} & -\frac{1}{10w^3} & \frac{1}{5w^3} & 0 \\
-\frac{1}{5w^3} & -\frac{1}{5w^3} & 0 & 0 & 0 & 0 & 0 & \frac{1}{5w^3} & \frac{1}{5w^3} & \frac{1}{5w^3} \\
-\frac{1}{70w^3} & \frac{1}{35w^3} & 0 & 0 & 0 & 0 & 0 & -\frac{1}{35w^3} & \frac{1}{70w^3} & \frac{1}{35w^3} \\
-\frac{1}{70w^3} & -\frac{1}{35w^3} & \frac{2}{35w^3} & \frac{1}{35w^3} & 0 & -\frac{1}{35w^3} & -\frac{2}{35w^3} & \frac{1}{35w^3} & \frac{1}{70w^3} & 0 \\
-\frac{1}{35w^2} & \frac{2}{35w^2} & \frac{2}{35w^2} & -\frac{1}{35w^2} & -\frac{2}{35w^2} & -\frac{1}{35w^2} & \frac{2}{35w^2} & \frac{2}{35w^2} & -\frac{1}{35w^2} & -\frac{2}{35w^2} \\
-\frac{1}{35w^2} & -\frac{1}{35w^2} & -\frac{2}{35w^2} & -\frac{2}{35w^2} & -\frac{2}{35w^2} & -\frac{2}{35w^2} & -\frac{2}{35w^2} & -\frac{1}{35w^2} & -\frac{1}{35w^2} & -\frac{1}{35w^2} \\
\frac{1}{100w^2} & \frac{1}{50w^2} & 0 & 0 & 0 & 0 & 0 & \frac{1}{50w^2} & \frac{1}{100w^2} & 0 \\
\frac{31}{210w} & \frac{1}{84w} & -\frac{17}{420w} & -\frac{17}{105w} & 0 & \frac{17}{105w} & \frac{17}{420w} & -\frac{1}{84w} & -\frac{31}{210w} & 0 \\
\frac{31}{210w} & \frac{11}{105w} & 0 & 0 & 0 & 0 & 0 & -\frac{11}{105w} & -\frac{31}{210w} & -\frac{17}{105w} \\
\frac{17}{175} & \frac{2}{175} & \frac{1}{25} & \frac{22}{175} & \frac{27}{175} & \frac{22}{175} & \frac{1}{25} & \frac{2}{175} & \frac{17}{175} & \frac{22}{175}
\end{Vmatrix} \tag{11}$$

$$\begin{Vmatrix}
-\frac{1}{5w^3} & \frac{1}{10w^3} & -\frac{1}{10w^3} & \frac{1}{5w^3} & 0 & -\frac{1}{5w^3} & \frac{1}{10w^3} \\
\frac{1}{5w^3} & \frac{1}{5w^3} & -\frac{1}{10w^3} & -\frac{1}{10w^3} & -\frac{1}{10w^3} & -\frac{1}{10w^3} & -\frac{1}{10w^3} \\
\frac{1}{70w^3} & -\frac{1}{35w^3} & -\frac{2}{35w^3} & \frac{1}{35w^3} & \frac{2}{35w^3} & \frac{1}{35w^3} & -\frac{2}{35w^3} \\
-\frac{1}{70w^3} & -\frac{1}{35w^3} & -\frac{2}{35w^3} & -\frac{1}{35w^3} & 0 & \frac{1}{35w^3} & \frac{2}{35w^3} \\
-\frac{1}{35w^2} & \frac{2}{35w^2} & \frac{2}{35w^2} & -\frac{1}{35w^2} & -\frac{2}{35w^2} & -\frac{1}{35w^2} & \frac{2}{35w^2} \\
-\frac{1}{35w^2} & -\frac{1}{35w^2} & \frac{2}{35w^2} & \frac{2}{35w^2} & \frac{2}{35w^2} & \frac{2}{35w^2} & \frac{2}{35w^2} \\
-\frac{1}{100w^2} & -\frac{1}{50w^2} & \frac{1}{25w^2} & \frac{1}{50w^2} & 0 & -\frac{1}{50w^2} & -\frac{1}{25w^2} \\
\frac{31}{210w} & \frac{1}{84w} & \frac{31}{420w} & -\frac{11}{105w} & 0 & \frac{11}{105w} & -\frac{31}{420w} \\
-\frac{31}{210w} & -\frac{11}{105w} & \frac{31}{420w} & -\frac{1}{84w} & -\frac{17}{420w} & -\frac{1}{84w} & \frac{31}{420w} \\
\frac{17}{175} & \frac{2}{175} & -\frac{13}{175} & \frac{2}{175} & \frac{1}{25} & \frac{2}{175} & -\frac{13}{175}
\end{Vmatrix}$$

Through simple algebraic operations, we can obtain the formulae for the partial derivatives of elevation:

$$a=\frac{1}{10w^3}[z_5+z_{10}+z_{15}+z_{20}+z_{25}-z_1-z_6-z_{11}-z_{16}-z_{21}+ 2(z_2+z_7+z_{12}+z_{17}+z_{22}-z_4-z_9-z_{14}-z_{19}-z_{24})] \tag{12}$$

$$d=\frac{1}{10w^3}[z_1+z_2+z_3+z_4+z_5-z_{21}-z_{22}-z_{23}-z_{24}-z_{25}+ 2(z_{16}+z_{17}+z_{18}+z_{19}+z_{20}-z_6-z_7-z_8-z_9-z_{10})] \tag{13}$$

$$b=\frac{1}{70w^3}[z_{17}+z_{19}-z_7-z_9+4(z_1+z_5+z_{23}-z_3-z_{21}-z_{25})+ 2(z_6+z_{10}+z_{18}+z_{22}+z_{24}-z_2-z_4-z_8-z_{16}-z_{20})] \tag{14}$$

$$c=\frac{1}{70w^3}[z_7+z_{17}-z_9-z_{19}+4(z_5+z_{11}+z_{25}-z_1-z_{15}-z_{21})+ 2(z_4+z_6+z_{12}+z_{16}+z_{24}-z_2-z_{10}-z_{14}-z_{20}-z_{22})] \tag{15}$$

$$r=\frac{1}{35w^2}[2(z_1+z_5+z_6+z_{10}+z_{11}+z_{15}+z_{16}+z_{20}+z_{21}+z_{25})- 2(z_3+z_8+z_{13}+z_{18}+z_{23})-z_2-z_4-z_7-z_9-z_{12}-z_{14}-z_{17}-z_{19}-z_{22}-z_{24}] \tag{16}$$

$$t=\frac{1}{35w^2}[2(z_1+z_2+z_3+z_4+z_5+z_{21}+z_{22}+z_{23}+z_{24}+z_{25})- 2(z_{11}+z_{12}+z_{13}+z_{14}+z_{15})-z_6-z_7-z_8-z_9-z_{10}-z_{16}-z_{17}-z_{18}-z_{19}-z_{20}] \tag{17}$$

$$s=\frac{1}{100w^2}[z_9+z_{17}-z_7-z_{19}+4(z_5+z_{21}-z_1-z_{25})+ 2(z_4+z_{10}+z_{16}+z_{22}-z_2-z_6-z_{20}-z_{24})] \tag{18}$$

$$p=\frac{1}{420w}\{44(z_4+z_{24}-z_2-z_{22})+31[z_1+z_{21}-z_5-z_{25}+2(z_9+z_{19}-z_7-z_{17})]+ 17[z_{15}-z_{11}+4(z_{14}-z_{12})]+5(z_{10}+z_{20}-z_6-z_{16})\} \tag{19}$$

$$q=\frac{1}{420w}\{44(z_6+z_{10}-z_{16}-z_{20})+31[z_{21}+z_{25}-z_1-z_5+2(z_7+z_9-z_{17}-z_{19})]+ 17[z_3-z_{23}+4(z_8-z_{18})]+5(z_2+z_4-z_{22}-z_{24})\} \tag{20}$$

We do not present a formula for the term u, since it is not used in calculations.

The formulae deduced (12–20) can be used to compute not only the derivation function but any local topographic variable, such as slope gradient, aspect, and land surface curvatures as well.

3. Calculation accuracy of the partial derivatives and derivation function

Let us compare the calculation accuracy of expressions of the second- and first-order partial derivatives related to the third-order polynomial (16–20) and those

related to the second-order polynomial (A7–A11) in terms of root mean square error (RMSE) of a function F of measured variables (m_F):

$$m_F = \sqrt{\left(\frac{\partial F}{\partial x}\right)_0^2 m_x^2 + \left(\frac{\partial F}{\partial y}\right)_0^2 m_y^2 + \ldots + \left(\frac{\partial F}{\partial u}\right)_0^2 m_u^2} \tag{21}$$

where x, y, …, u are measured arguments of F, and m_x, m_y, …, m_u are RMSE of x, y, …, u, correspondingly. For the Evans method, Florinsky (1998a) developed formulae of RMSE of r, t, s, p, and q (m_r, m_t, m_s, m_p, and m_q, respectively – table 1). In a similar manner, let us produce formulae of m_r, m_t, m_s, m_p, and m_q for expressions (16–20), as well as formulae of RMSE of a, d, b, and c for expressions (12–15) (m_a, m_d, m_b and m_c, respectively). Considering $m_{z_1} = m_{z_2} = \ldots = m_{z_{25}} = m_z$, where m_{z_i} is RMSE of z_i, we obtained the required formulae (table 1).

Let us compare the formulae of m_r, m_t, m_s, m_p and m_q related to the two polynomials (table 1). RMSE of partial derivatives of elevation is in direct proportion to m_z and in inverse (linear and quadratic) proportions to w. Under the same w and m_z, the equations of r, t, and s, related to the third-order polynomial, result in significantly lower values of RMSE than those related to the second-order polynomial (table 1). Indeed, m_r and m_t for equations (16 and 17) are almost 6 times less than those for equations (A7 and A8). m_s for equation (18) is 5 times less than that for equation (A9). m_p and m_q for equations (19 and 20) are a mere 10% higher than those for equations (A10 and A11) (table 1). This means that in derivating local topographic variables, the method developed can provide higher accuracy than the Evans method.

In a similar manner, let us develop a RMSE formula for T (m_T). To simplify the presentation of the formula, let us define five compound terms, A1 … A5, and rewrite equation (4) as

$$T = A_1(A_2 + A_3A_4A_5) \tag{22}$$

where

$$A_1 = \frac{1}{\sqrt{(p^2+q^2)^3(1+p^2+q^2)}} \tag{23a}$$

$$A_2 = q^3a - 3pq^2b + 3p^2qc - p^3d \tag{23b}$$

Table 1. RMSE of partial derivatives calculated by the Evans method (Florinsky 1998a) and the proposed method.

RMSE	The second-order polynomial, the 3×3 window	The third-order polynomial, the 5×5 window
m_p and m_q	$\frac{m_z}{\sqrt{6}w}$	$\sqrt{\frac{527}{70}}\frac{m_z}{6w}$
m_r and m_t	$\frac{\sqrt{2}m_z}{w^2}$	$\sqrt{\frac{2}{35}}\frac{m_z}{w^2}$
m_s	$\frac{m_z}{2w^2}$	$\frac{m_z}{10w^2}$
m_a and m_d	–	$\frac{m_z}{\sqrt{2}w^3}$
m_b and m_c	–	$\frac{m_z}{\sqrt{35}w^3}$

$$A_3 = q^2 r - 2pqs + p^2 t \tag{23c}$$

$$A_4 = \frac{2 + 3p^2 + 3q^2}{(p^2 + q^2)(1 + p^2 + q^2)} \tag{23d}$$

$$A_5 = pq(t - r) + s\left(p^2 - q^2\right) \tag{23e}$$

In this case,

$$m_T = \sqrt{m_{A_1}^2 \left(A_2^2 + 2A_2A_3A_4A_5 + A_3^2A_4^2A_5^2\right) + A_1^2\left[m_{A_2}^2 + A_5^2\left(A_4^2 m_{A_3}^2 + A_3^2 m_{A_4}^2\right) + A_3^2A_4^2 m_{A_5}^2\right]} \tag{24}$$

where m_{A_i} are RMSE of the terms A_i. Considering $m_p = m_q$, $m_r = m_t$, $m_a = m_d$, and $m_b = m_c$ (table 1), expressions for m_{A_i} take the following forms:

$$m_{A_1}^2 = m_p^2 \frac{\left(3 + 4p^2 + 4q^2\right)^2}{(p^2 + q^2)^4 (1 + p^2 + q^2)^3} \tag{25a}$$

$$\begin{aligned} m_{A_2}^2 = {} & 9m_p^2\left[q^4\left(a^2 + b^2\right) + p^4\left(c^2 + d^2\right) + 2p^2q^2\left\{2\left(b^2 + c^2\right) + ac + bd\right\} - \right. \\ & \left. 4pq\left\{q^2 b(a + c) + p^2 c(b + d)\right\}\right] + m_a^2\left(p^6 + q^6\right) + 9m_b^2 p^2 q^2\left(p^2 + q^2\right) \end{aligned} \tag{25b}$$

$$m_{A_3}^2 = 4m_p^2\left[p^2\left(t^2 + s^2\right) - 2pqs(r + t) + q^2\left(r^2 + s^2\right)\right] + m_r^2\left(p^4 + q^4\right) + 4m_s^2 p^2 q^2 \tag{25c}$$

$$m_{A_4}^2 = 4m_p^2 \frac{\left[p^2\left(4 + 3p^2\right) + q^2\left(4 + 3q^2\right) + 6p^2q^2 + 2\right]^2}{(p^2 + q^2)^3 (1 + p^2 + q^2)^4} \tag{25d}$$

$$m_{A_5}^2 = m_p^2\left(p^2 + q^2\right)\left[4s^2 + (t - r)^2\right] + 2m_r^2 p^2 q^2 + m_s^2\left(p^2 - q^2\right)^2 \tag{25e}$$

Development of the formulae was carried out with the software Maple V Release 5.0 (© Waterloo Maple Inc., 1981–1997).

4. Materials and methods

To exemplify application of the method developed, we used a portion of a DEM of North Caucasus, Russia (Florinsky 2002). An irregular DEM was compiled by digitising a topographic map with contour interval of 50 m (Central Board of Geodesy and Cartography 1968). The area selected measures about 133 by 100 km including the middle part of the Kuma River basin. The irregular DEM included 2571 points.

Using the Delaunay triangulation and a piecewise quadric polynomial interpolation with matching derivatives along triangle edges (Watson 1992), we produced a square-gridded DEM with a grid size of 300 m (figure 2). To reduce high frequency noise in the DEM, we applied three iterations of smoothing to the DEM using the 3×3 window with linear inverse distance weights.

4.1 *Testing the method developed*

Digital models of k_h (figure 3), T (figure 4(*a*)), and m_T (figure 5) were derived from the smoothed DEM using the method developed. Combining digital models of T

Figure 2. Elevation map for the North Caucasus study area.

(figure 4(*a*)) and k_h (figure 3), we delineated loci of positive (figure 4(*b*)) and negative (figure 4(*c*)) extreme curvature of the topographic surface.

To compare accuracies of the method developed and the Evans method, we carried out the following procedures. First, we derived a digital model of k_h from the

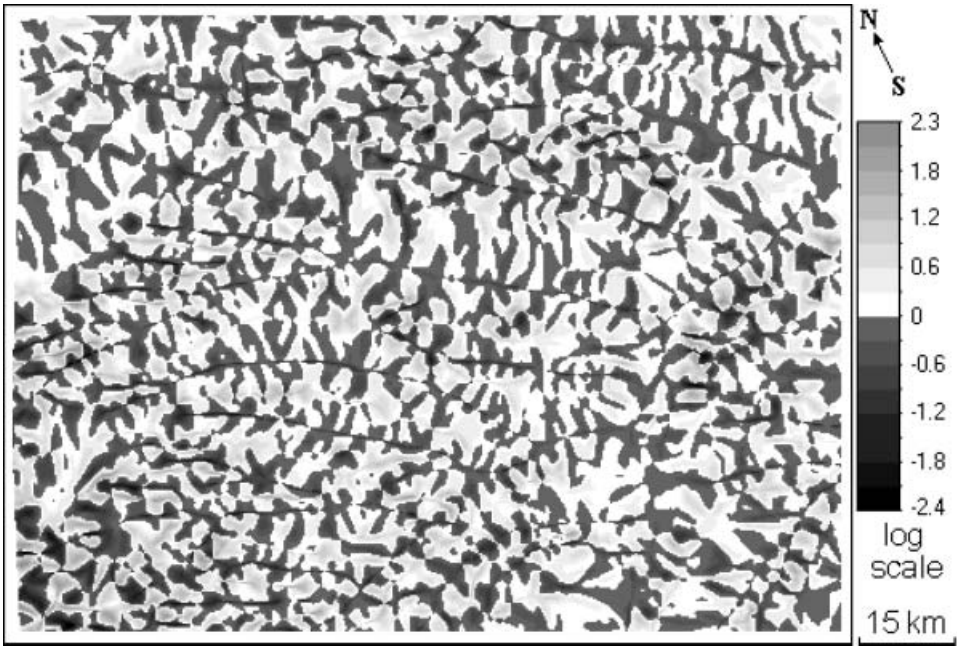

Figure 3. Map of horizontal curvature.

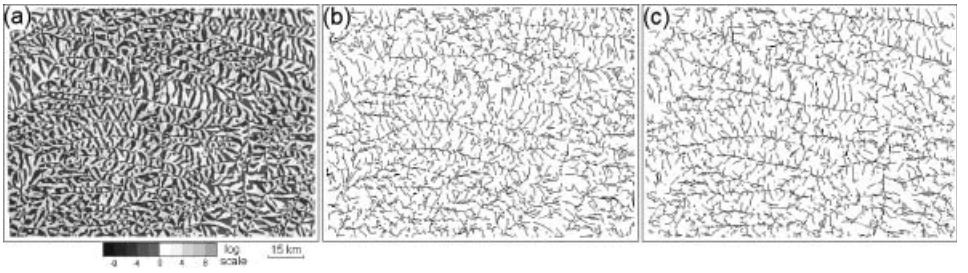

Figure 4. Maps of the derivation function: (*a*) spatial distribution of T values, (*b*) zero values of T within divergence areas – the locus of positive extreme curvature of the land surface, (*c*) zero values of T within convergence areas – the locus of negative extreme curvature of the land surface.

smoothed DEM by the Evans method (Appendix B). Second, the difference between the two k_h models (Δk_h) was calculated (figure 6(*a*)). Third, we visually analysed patterns of both k_h maps (figure 6(*b*) and (*c*)). Fourth, we performed an analysis of statistical distributions of Δk_h and both k_h values as well as the Kolmogorov-Smirnov test for statistical difference between the two distributions of k_h (figure 7). We used samples each including 1376 points (regular matrices 43×32 with the grid size of 3000 m extracted from related digital models).

It is undesirable to map a local topographic variable, such as k_h, with an equal-step quantification of its values. As a rule, this leads to information loss due to the large dynamic range of a digital model. To gain a better representation and understanding of patterns of k_h, Δk_h, T, and m_T maps, digital models of these

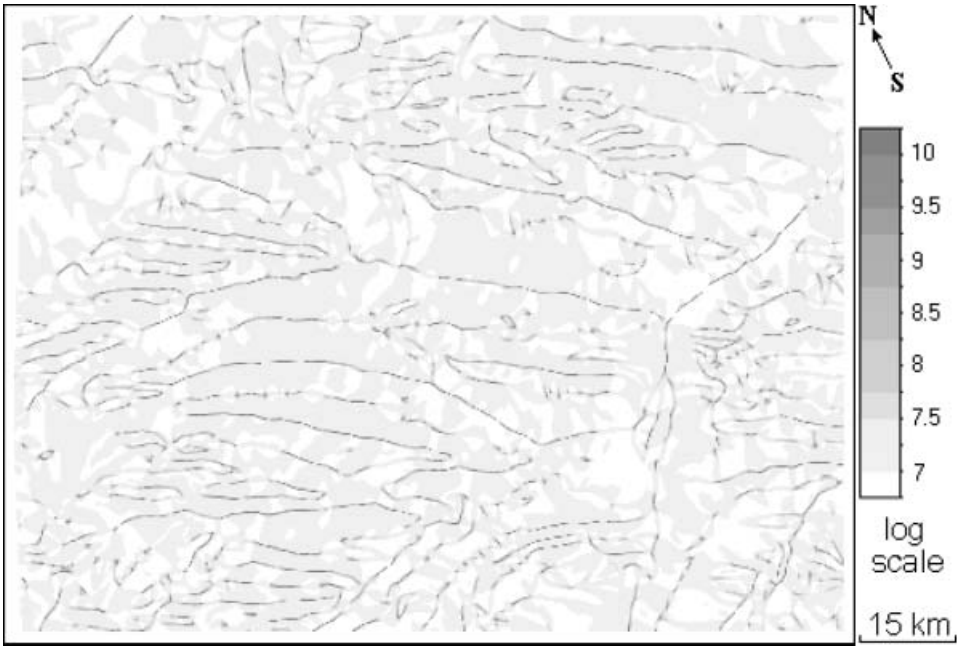

Figure 5. Map of RMSE of the derivation function.

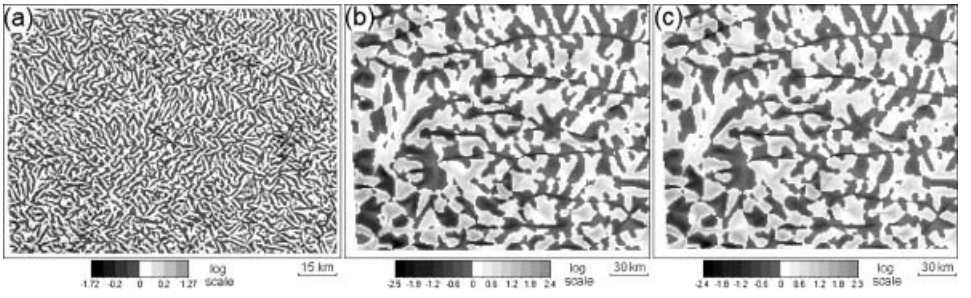

Figure 6. Horizontal curvature derived by two methods: (*a*) Δk_h map, (*b*) enlarged lower left portion of the k_h map derived by the Evans method, (*c*) enlarged lower left portion of the k_h map derived by the method developed.

variables were logarithmically transformed (Shary *et al.* 2002):

$$\Theta' = \mathrm{sign}(\Theta) \cdot \ln(1 + 10^n |\Theta|) \tag{26}$$

where Θ represents k_h, Δk_h, T, and m_T; $n=5$ for k_h and Δk_h, and $n=10$ for T and m_T.

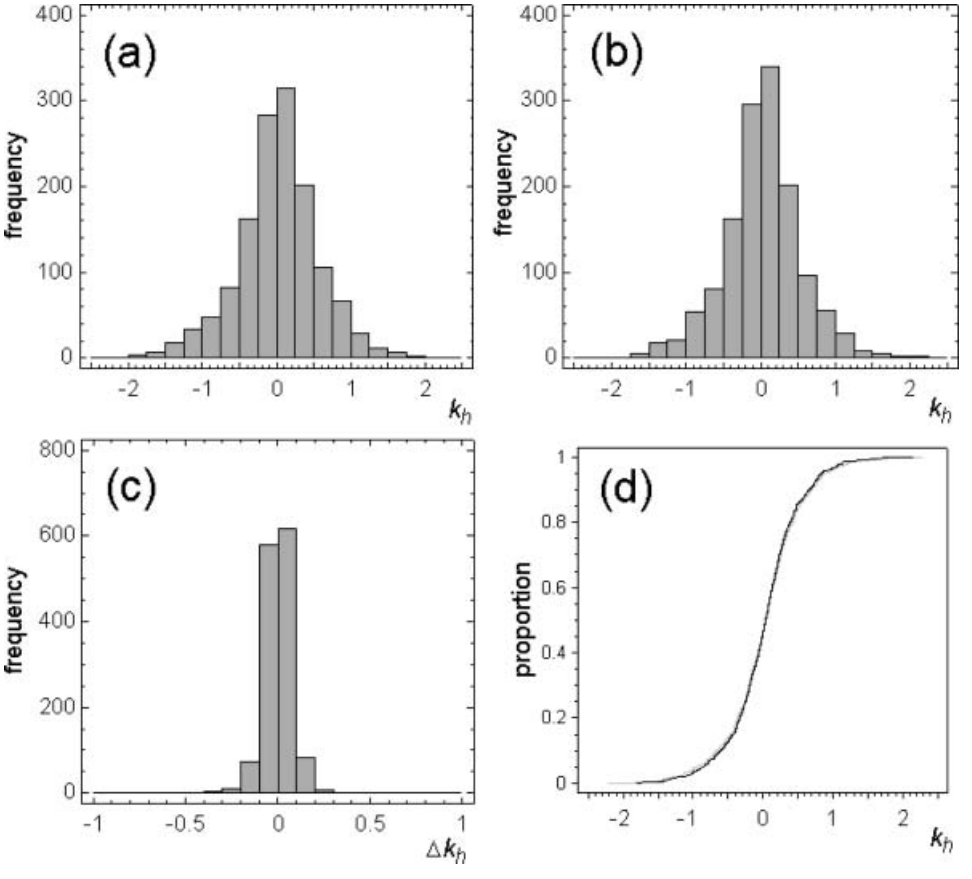

Figure 7. Statistical distribution of logarithmically transformed k_h values: (*a*) histogram for k_h derived by the Evans method, (*b*) histogram for k_h derived by the method developed, (*c*) histogram for Δk_h, (*d*) quantile plot for k_h derived by the Evans method (grey line) and the method developed (black line).

This form of transformation allows one to hold ranges of positive and negative values of a variable and scale them correctly (figures 3–6).

DEM interpolation and smoothing as well as calculation and mapping were done with LandLord 4.0 (Florinsky *et al.* 1995). Statistical analysis was carried out by Statgraphics Plus 3.0 (© Statistical Graphics Corp., 1994–1997).

4.2 *Detecting ridgelthalweg networks*

We did not attempt a comprehensive comparison of the performance of T mapping and previous algorithms in detecting ridge/thalweg networks. First, the loci of extreme curvature of the topographic surface, delineated by T mapping, are not equal to ridge and thalweg lines (section 1). Second, detailed comparisons of previous methods can be found elsewhere (Skidmore 1990, Tribe 1992, Gauch and Pizer 1993, López *et al.* 1999). To check a proposal of Shary and Stepanov (1991) that T mapping can be used to reveal ridge/thalweg networks, we compared maps of loci of positive and negative extreme curvature (figure 4(*b*) and (*c*)) with ridge/thalweg maps obtained using the software CatchmentSIM 1.29 (Ryan and Boyd 2003).

In this software, flats and pits can be removed from a DEM by the breaching algorithm of Jones (2002). In flow routing, a downslope flow angle is determined by a modified multiple direction algorithm (Lea 1992). Channel heads are detected using a catchment area threshold (Jones 2002). In a raster procedure, thalwegs are defined as pixels with catchment area values greater than the threshold. In a vector procedure, thalwegs are traced from each channel head, their intersections are recorded, and then thalweg ordering is calculated. Treating an inverted DEM, a ridge network may be constructed in the same way.

After elimination of pits and flats from the DEM, we produced two maps of ridges and thalwegs using CatchmentSIM. First, ridges and thalwegs were delineated by the raster procedure with a catchment area threshold of 25 pixels (figure 8(*a*)). Second, six orders of ridges and thalwegs were mapped by the vector procedure (figure 8(*b*)).

5. Results and discussion

5.1 *Detecting ridgelthalweg networks*

The map of T (figure 4(*a*)) includes all loci of extreme curvature of the topographic surface. They appear as borders between areas of positive and negative values of T

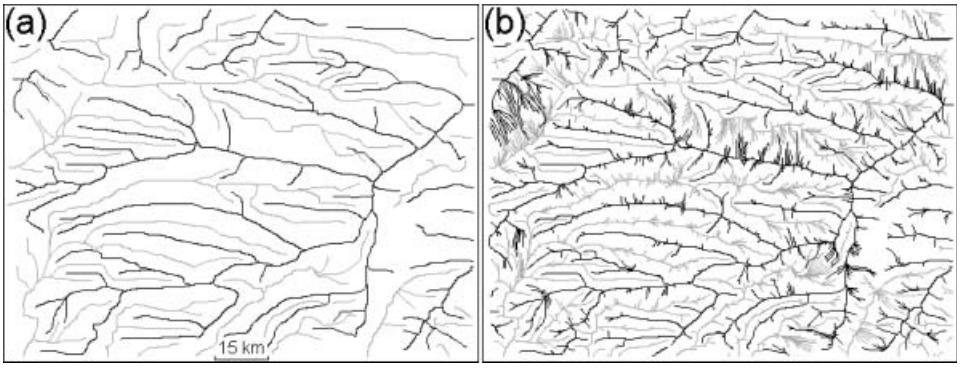

Figure 8. Ridge (grey) and thalweg (black) networks derived from the DEM using CatchmentSIM software, by (*a*) raster procedure; (*b*) vector procedure.

(light and dark patterns, correspondingly). The map of zero values of the derivation function located within areas of flow divergence ($T=0$ with $k_h>0$) displays the locus of positive extreme curvature (figure 4(*b*)). The map of zero values of the derivation function located within areas of flow convergence ($T=0$ with $k_h<0$) displays the locus of negative extreme curvature (figure 4(*c*)).

The m_T map (figure 5) displays the spatial distribution of the probability of error arising during calculations. The highest m_T values can be found along loci of extreme curvature. As with RMSE of curvatures (Florinsky 1998a), m_T values may be in excess of absolute maximal values of T (figure 5).

According to Shary and Stepanov (1991), the positive extreme curvature map (figure 4(*b*)) should display ridges and convex break lines, while the negative extreme curvature map (figure 4(*c*)) should represent thalwegs and concave break lines. However, even a cursory examination of the maps showed that they fail to detect these geomorphic lines correctly. This inference is supported by comparison with the maps of ridge/thalweg networks delineated using regional logistic approaches (figure 8). The main problem is that loci of extreme curvature are interrupted in many places (figure 4(*b*) and (*c*)). This can be caused by interpolation and smoothing errors, the remains of the high frequency noise of the DEM, and loci of special points, viz. local maxima and minima, saddles, and minor flat horizontal areas.

Therefore, in terms of ridge/thalweg detection, T mapping is marked by the following disadvantages. First, once again, loci of extreme curvature may only partially define thalweg/ridge lines (section 1). Second, the calculation of partial derivatives is sensitive to errors and noise existing copiously in a DEM (Florinsky 2002). Third, T mapping cannot reveal thalweg/ridge networks as hierarchical structures of tributary orders. These may testify that T mapping cannot substitute regional logistic algorithms. To claim this unambiguously, considering the limitations of the DEM interpolated from the contour map, one should carry out further tests of T-based revealing of thalweg/ridge networks using more detailed non-interpolated DEMs derived from LiDAR or SRTM data.

5.2 *Testing the method developed*

As a tool to compute local topographic variables, the method developed shares a common trait with the Evans approach (Appendix B): the polynomial (5) is approximated to elevation values of the 5×5 window rather than passing exactly through them. This leads to a local denoising that may enhance the calculation of derivatives and local topographic variables because they are responsive to a high frequency component of a signal (Florinsky 2002). However, Wood (1996) supposed that calculation of derivatives fitting the third and higher order polynomials to $n \times n$ windows, where $n>3$, can lead to an undue generalisation of the surface.

This is not necessarily the case. Comparing k_h maps derived by two methods (figure 6(*c*) and (*d*)), one can see that local changes in map patterns enclose from one to about five pixels. This is a level of denoising rather than generalisation. One can find the same level of changes in the k_h dynamic range: it was [−2.55/2.44] and [−2.49/2.31] for the Evans method and for the developed method, correspondingly (figure 6(*c*) and (*d*)). Thus, the change in the k_h dynamic range was only about 4%. This is an insignificant alteration. The map of Δk_h represents a complex picture for the spatial distribution of changes in k_h values (figure 6(*a*)). However, most changes

were in the range from −0.1 to 0.1 (figure 7(*c*)). Again, this is 4% of the dynamic range of k_h derived by the Evans method. Histograms of the two k_h samples are very similar (figure 7(*a*) and (*b*)). Results of the Kolmogorov-Smirnov test applied to the two k_h samples are as follows: the estimated overall statistic DN=0.025, the two-sided large sample K-S statistic is 0.67, and P value=0.77. Thus, there is no statistically significant difference between the two distributions at the 95% confidence level. The quantile plot demonstrates this: curves for the two k_h samples coincide very closely (figure 7(*d*)). Therefore, the method developed provides additional denoising of a DEM without an undue generalisation of the surface.

Brief mention should be made of two secondary features of the method proposed. First, formulae (16–20) are longer than the related expressions (A7–A11). Therefore, the method works slower than the Evans method. However, this is not a critical feature considering the efficiency of contemporary computers. Second, since all functions (partial derivatives and local topographic attributes) are calculated for the central point of the moving window (figure 1), they cannot be calculated for two border rows and two border columns on each side of the DEM matrix. In the Evans method, functions cannot be derived for the border rows and columns.

6. Conclusions

We deduced formulae to compute the third-, second- and first-order partial derivatives from a DEM fitting the third-order polynomial to the 5×5 window. The polynomial is approximated to elevation values of the window rather than passing exactly through them. This leads to a local denoising that may enhance the calculation of partial derivatives. The new method can be used to compute any local topographic variable, such as slope gradient, aspect, land surface curvatures, derivation function, etc. Compared to the Evans method, the method developed allows one to derive more accurate models of topographic attributes.

This study demonstrated that T mapping may not substitute regional logistic algorithms to detect ridge/thalweg networks. However, the third-order partial derivatives can be used in digital terrain analysis. In particular, there were proposals to consider them in landform classifications (Lastochkin 1987, Jenčo 1992, Minár and Evans 2008). The method developed can be used to implement those ideas. One can also utilise digital models of T, among other topographic attributes, in studying and modelling relationships between topography and soil or plant properties.

Acknowledgments

The author thanks three anonymous reviewers for useful criticism.

References

BAND, L.E., 1986, Topographic partition of watersheds with digital elevation models. *Water Resources Research*, **22**, pp. 15–24.

BJERHAMMAR, A., 1973, *Theory of Errors and Generalized Matrix Inverses* (Amsterdam: Elsevier).

BOUSSINESQ, M.J., 1871, Sur une propriété remarquable des points où les lignes de plus grand pente d'une surface ont leurs plans osculateurs verticaux, et sur la différence qui existe généralement, à la surface de la terre, entre les lignes de faîte ou de thalweg et celles le long desquelles la pente du sol est un minimum. *Comptes Rendus Hebdomadaires des Séances de l'Académie des Sciences*, **73**, pp. 1368–1371.

BRETON DE CHAMP, M., 1877, Mémoire sur les lignes de faîte et de thalweg que l'on est conduit à considérer en topographie. *Journal de Mathématique Pure et Appliquées, Series 3*, **3**, pp. 99–114.

CAYLEY, A., 1859, On contour and slope lines. *The London, Edinburgh and Dublin Philosophical Magazine and Journal of Science, Ser. 4*, **18**, pp. 264–268.

CENTRAL BOARD OF GEODESY AND CARTOGRAPHY, 1968, *Topographic Map, scale 1:1 000 000, Chart L–38 (Pyatigorsk)* (Moscow: Central Board of Geodesy and Cartography) (in Russian).

CHANG, Y.C., SONG, G.S. and HSU, S.K., 1998, Automatic extraction of ridge and valley axes using the profile recognition and polygon-breaking algorithm. *Computers and Geosciences*, **24**, pp. 83–93.

DE SAINT-VENANT, M., 1852, Surfaces à plus grande pente constitutées sur des lignes courbes. *Extraits des Procès-Verbaux des Séances de la Société Philomathique de Paris, Series 5*, **17**, pp. 24–30.

DOUGLAS, D.H., 1986, Experiments to locate ridges and channels to create a new type of digital elevation model. *Cartographica*, **23**, pp. 29–61.

EBERLY, D., GARDNER, R., MORSE, B., PIZER, S. and SCHARLACH, C., 1994, Ridges for image analysis. *Journal of Mathematical Imaging and Vision*, **4**, pp. 351–371.

EVANS, I.S., 1979, An integrated system of terrain analysis and slope mapping. Final report on grant DA-ERO-591-73-G0040 (Durham: University of Durham).

FIKHTENGOLTS, G.M., 1966, *A Course in Differential and Integral Calculus, Vol. 1*, 6th edtion (Moscow: Nauka) (in Russian).

FLORINSKY, I.V., 1998a, Accuracy of local topographic variables derived from digital elevation models. *International Journal of Geographical Information Science*, **12**, pp. 47–61.

FLORINSKY, I.V., 1998b, Combined analysis of digital terrain models and remotely sensed data in landscape investigations. *Progress in Physical Geography*, **22**, pp. 33–60.

FLORINSKY, I.V., 2002, Errors of signal processing in digital terrain modelling. *International Journal of Geographical Information Science*, **16**, pp. 475–501.

FLORINSKY, I.V., GROKHLINA, T.I. and MIKHAILOVA, N.L., 1995, Landlord 2.0: The software for analysis and mapping of geometrical characteristics of relief. *Geodesiya i Cartographiya*, **5**, pp. 46–51 (in Russian).

GAUCH, J.M. and PIZER, S.M., 1993, Multiresolution analysis of ridges and valleys in gray-scale images. *IEEE Transactions on Pattern Analysis and Machine Intelligence*, **15**, pp. 635–646.

JENČO, M., 1992, The morphometric analysis of georelief in terms of a theoretical conception of the complex digital model of georelief. *Acta Facultatis Rerum Naturalium Universitatis Comenianae, Geographica*, **33**, pp. 133–151.

JONES, R., 2002, Algorithms for using a DEM for mapping catchment areas of stream sediment samples. *Computers and Geosciences*, **28**, pp. 1051–1060.

JORDAN, M.C., 1872, Sur les lignes de faîte et de thalweg. *Comptes Rendus Hebdomadaires des Séances de l'Académie des Sciences*, **74**, pp. 1457–1459.

HARALICK, R., 1983, Ridges and valleys on digital images. *Computer Vision, Graphics, and Image Processing*, **22**, pp. 28–38.

KOENDERINK, J.J. and VAN DOORN, A.J., 1993, Local features of smooth shapes: Ridges and courses. *Proceedings of SPIE*, **2013**, pp. 2–13.

KWEON, I.S. and KANADE, T., 1994, Extracting topographic terrain features from elevation maps. *CVGIP: Image Understanding*, **59**, pp. 171–182.

LANG, S., 1996, *Calculus of Several Variables*, 3rd revised edtion (New York: Springer).

LASTOCHKIN, A.N., 1987, *Morphodynamical Analysis* (Leningrad: Nedra) (in Russian).

LEA, N.L., 1992, An aspect driven kinematic routing algorithm. In: *Overland Flow: Hydraulics and Erosion Mechanics*, A.J. Parsons and A.D. Abrahams (Eds), pp. 393–407 (New York: Chapman and Hall).

López, A.M. and Serrat, J., 1996, Tracing crease curves by solving a system of differential equations. *Lecture Notes in Computer Science*, **1064**, pp. 241–250.

López, A.M., Lumbreras, F. and Serrat, J., 1998, Creaseness from level set extrinsic curvature. *Lecture Notes in Computer Science*, **1407**, pp. 156–169.

López, A.M., Lumbreras, F., Serrat, J. and Villanueva, J.J., 1999, Evaluation of methods for ridge and valley detection. *IEEE Transactions on Pattern Analysis and Machine Intelligence*, **21**, pp. 327–335.

Maintz, J.B.A., van den Elsen, P.A. and Viergever, M.A., 1996, Evaluation of ridge seeking operators for multimodality medical image matching. *IEEE Transactions on Pattern Analysis and Machine Intelligence*, **18**, pp. 353–365.

Mark, D.M., 1984, Automated detection of drainage networks from digital elevation models. *Cartographica*, **21**, pp. 168–178.

Maxwell, J.C., 1870, On hills and dales. *The London, Edinburgh and Dublin Philosophical Magazine and Journal of Science, Ser. 4*, **40**, pp. 421–427.

Meisels, A., Raizman, S. and Karnieli, A., 1995, Skeletonizing a DEM into a drainage network. *Computers and Geosciences*, **21**, pp. 187–196.

Minár, J. and Evans, I.S., 2008, Elementary forms for land surface segmentation: The theoretical basis of terrain analysis and geomorphological mapping. *Geomorphology*, **95**, pp. 236–259.

O'Callaghan, J.F. and Mark, D.M., 1984, The extraction of drainage networks from digital elevation data. *Computer Vision, Graphics, and Image Processing*, **28**, pp. 323–344.

Rieger, J., 1997, Topographical properties of generic images. *International Journal of Computer Vision*, **23**, pp. 79–92.

Rothe, R., 1915, Zum problem des talwegs. *Sitzungsberichte der Berliner Mathematischen Gesellschaft*, **14**, pp. 51–68.

Ryan, C. and Boyd, M., 2003, CatchmentSIM: A new GIS tool for topographic geo-computation and hydrologic modelling. In M. Boyd, J. Ball, M. Babister and J. Green (Eds), *Proceedings of the 28th International Hydrology and Water Resources Symposium*, Vol. 1, pp. 35–42 (Wollongong: the Institution of Engineers).

Schmidt, J., Evans, I.S. and Brinkmann, J., 2003, Comparison of polynomial models for land surface curvature calculation. *International Journal of Geographical Information Science*, **17**, pp. 797–814.

Shary, P.A., 1991, The second derivative topographic method. In: *The Geometry of the Earth Surface Structures*, I.N. Stepanov, (Ed), pp. 30–60 (Pushchino: Pushchino Research Centre Press) (in Russian).

Shary, P.A. and Stepanov, I.N., 1991, On the second derivative method in geology. *Doklady Academii Nauk SSSR*, **319**, pp. 456–460, (in Russian).

Shary, P.A., Sharaya, L.S. and Mitusov, A.V., 2002, Fundamental quantitative methods of land surface analysis. *Geoderma*, **107**, pp. 1–32.

Skidmore, A.K., 1990, Terrain position as mapped from a gridded digital elevation model. *International Journal of Geographical Information Systems*, **4**, pp. 33–49.

Steger, C., 1999, Extraction of watersheds from DTM and images with subpixel precision. *International Archives of Photogrammetry and Remote Sensing*, **32**, Part 3-2W5, pp. 55–60.

Tribe, A., 1992, Automated recognition of valley lines and drainage networks from grid digital elevation models: A review and a new method. *Journal of Hydrology*, **139**, pp. 263–293.

Watson, D., 1992, *Contouring: A Guide to the Analysis and Display of Spatial Data* (Oxford: Pergamon Press).

Wood, J.D., 1996, *The Geomorphological Characterisation of Digital Elevation Models*, PhD thesis, University of Leicester, Leicester, UK.

Zevenbergen, L.W. and Thorne, C.R., 1987, Quantitative analysis of land surface topography. *Earth Surface Processes and Landforms*, **12**, pp. 47–56.

Appendix A. Deduction of the equation for the derivation function

From equations (1) and (2) follows

$$\frac{\mathrm{d}k_h}{\mathrm{d}\xi}=\frac{\partial k_h}{\partial p}\frac{\partial p}{\partial \xi}+\frac{\partial k_h}{\partial q}\frac{\partial q}{\partial \xi}+\frac{\partial k_h}{\partial r}\frac{\partial r}{\partial \xi}+\frac{\partial k_h}{\partial s}\frac{\partial s}{\partial \xi}+\frac{\partial k_h}{\partial t}\frac{\partial t}{\partial \xi} \tag{A1}$$

Considering equations (3), it is clear that

$$\frac{\partial p}{\partial \xi}=\frac{\partial p}{\partial x}\frac{\partial x}{\partial \xi}+\frac{\partial p}{\partial y}\frac{\partial y}{\partial \xi}=r\frac{\partial x}{\partial \xi}+s\frac{\partial y}{\partial \xi} \tag{A2}$$

Similarly,

$$\frac{\partial q}{\partial \xi}=s\frac{\partial x}{\partial \xi}+t\frac{\partial y}{\partial \xi},\ \frac{\partial r}{\partial \xi}=a\frac{\partial x}{\partial \xi}+b\frac{\partial y}{\partial \xi},\ \frac{\partial s}{\partial \xi}=b\frac{\partial x}{\partial \xi}+c\frac{\partial y}{\partial \xi},\ \frac{\partial t}{\partial \xi}=c\frac{\partial x}{\partial \xi}+d\frac{\partial y}{\partial \xi} \tag{A3}$$

$$\frac{\partial x}{\partial \xi}=\pm\frac{-q}{\sqrt{p^2+q^2}},\quad \frac{\partial y}{\partial \xi}=\pm\frac{p}{\sqrt{p^2+q^2}} \tag{A4}$$

where the choice of a sign depends on the choice of a contour orientation (Shary 1991).

After differentiation, expression (A1) takes the form:

$$\begin{aligned}T=&\frac{sp-rq}{\sqrt{p^2+q^2}}\left[\frac{2(sq-tp)}{(p^2+q^2)\sqrt{1+p^2+q^2}}+\frac{2p\left(q^2r-2pqs+p^2t\right)}{\left(p^2+q^2\right)^2\sqrt{1+p^2+q^2}}+\frac{p\left(q^2r-2pqs+p^2t\right)}{(p^2+q^2)\sqrt{\left(1+p^2+q^2\right)^3}}\right]+\\&\frac{tp-sq}{\sqrt{p^2+q^2}}\left[\frac{2(sp-rq)}{(p^2+q^2)\sqrt{1+p^2+q^2}}+\frac{2q\left(q^2r-2pqs+p^2t\right)}{\left(p^2+q^2\right)^2\sqrt{1+p^2+q^2}}+\frac{q\left(q^2r-2pqs+p^2t\right)}{(p^2+q^2)\sqrt{\left(1+p^2+q^2\right)^3}}\right]+\\&\frac{q^2(qa-pb)}{\sqrt{\left(p^2+q^2\right)^3\left(1+p^2+q^2\right)}}-\frac{2pq(qb-pc)}{\sqrt{\left(p^2+q^2\right)^3\left(1+p^2+q^2\right)}}+\frac{p^2(qc-pd)}{\sqrt{\left(p^2+q^2\right)^3\left(1+p^2+q^2\right)}}\end{aligned} \tag{A5}$$

After simple algebraic operation, we obtain expression (4).

Appendix B. The Evans method

In the method of Evans (1979), the second-order polynomial

$$z=\frac{rx^2}{2}+\frac{ty^2}{2}+sxy+px+qy+u \tag{A6}$$

is fitted by the least squares method to the 3×3 square-spaced window with a grid size of w. Window points $(-w, w, z_1)$, $(0, w, z_2)$, (w, w, z_3), $(-w, 0, z_4)$, $(0, 0, z_5)$, $(w, 0, z_6)$, $(-w, -w, z_7)$, $(0, -w, z_8)$, and $(w, -w, z_9)$ are measured Cartesian co-ordinates and elevations of the land surface. As a result, one can estimate r, t, s, p, and q at the point $(0, 0, z_5)$ by the finite difference formulae:

$$r=\frac{z_1+z_3+z_4+z_6+z_7+z_9-2(z_2+z_5+z_8)}{3w^2} \tag{A7}$$

$$t = \frac{z_1 + z_2 + z_3 + z_7 + z_8 + z_9 - 2(z_4 + z_5 + z_6)}{3w^2} \tag{A8}$$

$$s = \frac{z_3 + z_7 - z_1 - z_9}{4w^2} \tag{A9}$$

$$p = \frac{z_3 + z_6 + z_9 - z_1 - z_4 - z_7}{6w} \tag{A10}$$

$$q = \frac{z_1 + z_2 + z_3 - z_7 - z_8 - z_9}{6w} \tag{A11}$$

Moving the 3×3 window along a DEM, one can calculate values of r, t, s, p, and q for all points of a DEM, except boundary points.